

Imaging Inhomogeneous Dielectric Targets Through an Innovative Multi-Scaling Inverse Scattering Approach

M. Salucci, A. Polo, and A. Massa

Abstract

In this work, an innovative approach for solving the fully non-linear inverse scattering problem (*ISP*) is presented. It is based on the integration of the iterative multi-scaling approach (*IMSA*) and a New Integral Equation (*NIE*) method. On the one hand, the *IMSA* enables a significant reduction of the ratio between problem unknowns and available/non-redundant data coming from scattered field observations. On the other hand, the *NIE* allows to reformulate the *IS* equations such that a lower non-linearity is yielded when tackling the retrieval of non-weak scatterers. The *IMSA-NIE* method is tested against a quite challenging *IS* problem concerned with the imaging of an *inhomogeneous* unknown target comprising different values of dielectric permittivity. Numerical results are shown to assess the effectiveness of the proposed method also with comparisons against competitive state-of-the-art methods.

Contents

1	List of Symbols	2
2	Numerical Assessment	3
2.1	“Inhomogeneous Square” Profile - Variation of SNR	3
2.1.1	Results	5
2.2	Observations	8

ELEDIA Research Center

1 List of Symbols

- $k = \frac{2\pi}{\lambda}$: Free-space wave-number;
- D : Investigation domain;
- L_D : Side of the investigation domain;
- $a = L_D \frac{\sqrt{2}}{2}$: Radius of the smallest circle containing D ;
- $\mathbf{r} = (x, y)$: Position vector;
- $\tau(\mathbf{r})$: Contrast function;
- $\varepsilon_r(\mathbf{r})$: Relative permittivity;
- ε_0 : Free-space permittivity;
- $\sigma(\mathbf{r})$: Conductivity;
- Ξ : Reconstruction error;
- V : Number of views/sources;
- φ^v : Direction of the v -th plane wave ($v = 1, \dots, V$);
- M : Number of measurement points;
- ρ : Radius of the measurement domain;
- N : Number of discretization cells inside D ;
- Γ : Number of degrees-of-freedom of the scattered field;
- U : Number of retrievable unknowns;
- η : *IMSA* Stopping threshold;
- S : Maximum number of *IMSA* iterations;
- $L^{(s)}$: Side of the region of interest (*RoI*) at the s -th *IMSA* step ($s = 1, \dots, S$);
- K : Number of singular values used by the *SOM* to retrieve the minimum-norm currents;
- α : Threshold for the adaptive selection of the number of singular values;
- χ_m : m -th Singular value of the scattering operator ($m = 1, \dots, M$);
- MF : Number of Fourier bases;
- β : *NIE* regularization parameter;
- γ : Multiplicative factor for the adaptive computation of β ;
- I : Number of iterations;

2 Numerical Assessment

2.1 “Inhomogeneous Square” Profile - Variation of SNR

Investigation domain (D)

- Side: $L_D = 3.0 [\lambda]$;

Measurement setup

- Views
 - Type: plane wave with unitary magnitude;
 - Frequency: $f = 300 [\text{MHz}]$;
 - Wavelength: $\lambda = 1.0 [\text{m}]$;
 - Number of $DOFs$: $\Gamma = 2ka = 2k \left(L_D \frac{\sqrt{2}}{2} \right) = 4 \frac{\pi}{\lambda} \left(L_D \frac{\sqrt{2}}{2} \right) \simeq 26.64$;
 - Number of views: $V = 27$;
 - Direction: $\varphi_v = (v - 1) \frac{360}{V}$; $v = 1, \dots, V$;
- Measurement points
 - Radius: $\rho = a = \left(L_D \frac{\sqrt{2}}{2} \right) = 2.12 [\lambda]$;
 - Number of probes: $M = 27$;
 - Location: $(x_m, y_m) = \left(\rho \cos \left((m - 1) \frac{2\pi}{M} \right), \rho \sin \left((m - 1) \frac{2\pi}{M} \right) \right)$; $m = 1, \dots, M$;

Scatterer

- Type: Inhomogeneous Square;
- Side: $L_{obj,out} = 0.9 [\lambda]$, $L_{obj,in} = 0.3 [\lambda]$;
- Barycenter: $(x_{obj}, y_{obj}) = (0.45, -0.45) [\lambda]$;
- Dielectric characteristics: $\varepsilon_{r,in} = 4.0$, $\varepsilon_{r,out} = 2.0$, $\sigma = 0.0 [\text{S/m}] \rightarrow \tau_{in} = 3.0$, $\tau_{out} = 1.0$;

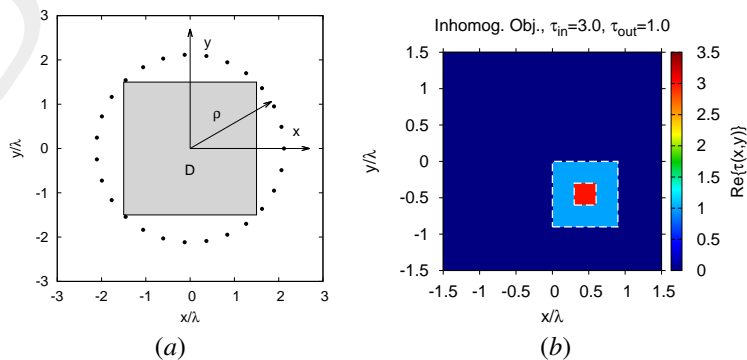


Figure 1: “Inhomogeneous Square” Profile, $\tau_{in} = 3.0$, $\tau_{out} = 1.0$ - (a) Imaging scenario and (b) actual dielectric profile.

Forward solver (*MoM*)

- Discretization: $N^{fwd} = 60 \times 60 = 3600$;
- Side of each cell: $l^{fwd} \simeq 0.05 [\lambda]$;

Inverse solver

1. *IMSA – SOM – NIE*

- Number of retrievable unknowns: $U = \frac{(2ka)^2}{2} = 4\pi^2 \left(\frac{L}{\lambda}\right)^2 = 355$;
- Discretization: $N^{IMSA} = 18 \times 18 = 324$;
- Side of each cell @ $s = 1$: $l_{s=1} = 0.17 [\lambda]$;
- Maximum number of steps: $S = 4$;
- *IMSA* stop criterion: adaptive ($\eta = 0.2$);
- Selection of the singular values: adaptive;
- Threshold for the adaptive selection of the number of singular values: $\alpha = 0.4$ (calibrated);
- Number of Fourier bases: $MF = \frac{\sqrt{N^{IMSA}}}{2} = 9$ (standard *SOM*);
- Selection of the *NIE* regularization parameter: adaptive;
- Multiplicative factor for the selection of the *NIE* regularization parameter: $\gamma = 0.5$ (calibrated);
- Number of iterations: $I = 100$.

2. *BARE – SOM – NIE*

- Discretization: $N^{BARE} = 30 \times 30 = 900$;
- Side of each cell: $l = 0.1 [\lambda]$;
- Number of singular values: $K = 15$ (non-adaptive);
- Number of Fourier bases: $MF = \frac{\sqrt{N^{BARE}}}{2} = 15$ (standard *SOM*);
- *NIE* regularization parameter: $\beta = 2.0$ (non-adaptive, calibrated);
- Number of iterations: $I = 100$.

3. *IMSA – SOM – CSI*

- Same parameters of *IMSA – SOM – NIE*;
- Threshold for the adaptive selection of the number of singular values: $\alpha = 0.7$;

4. *BARE – SOM – CSI*

- Same parameters of *BARE – SOM – NIE*;

Signal to noise ratio

- $SNR = \{10; 20; 40; 60\}$ [dB].

2.1.1 Results

IMSA – SOM – NIE vs. BARE – SOM – NIE: Final reconstructions

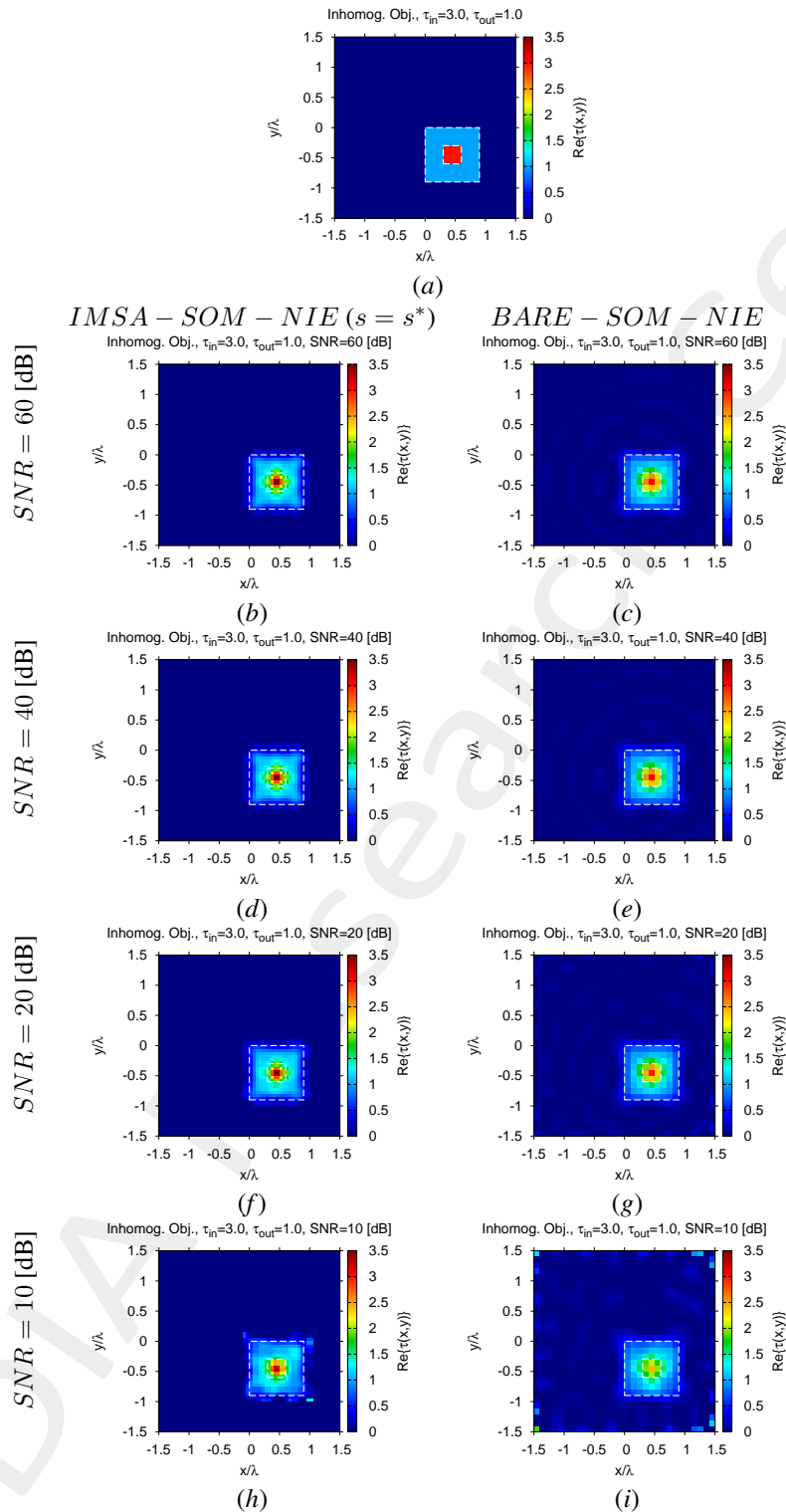


Figure 2: “Inhomogeneous Square” Profile, $\tau_{in} = 3.0$, $\tau_{out} = 1.0$ - (a) Actual and (b)-(i) retrieved contrast by the *IMSA – SOM – NIE* and *BARE – SOM – NIE* methods under several noise levels.

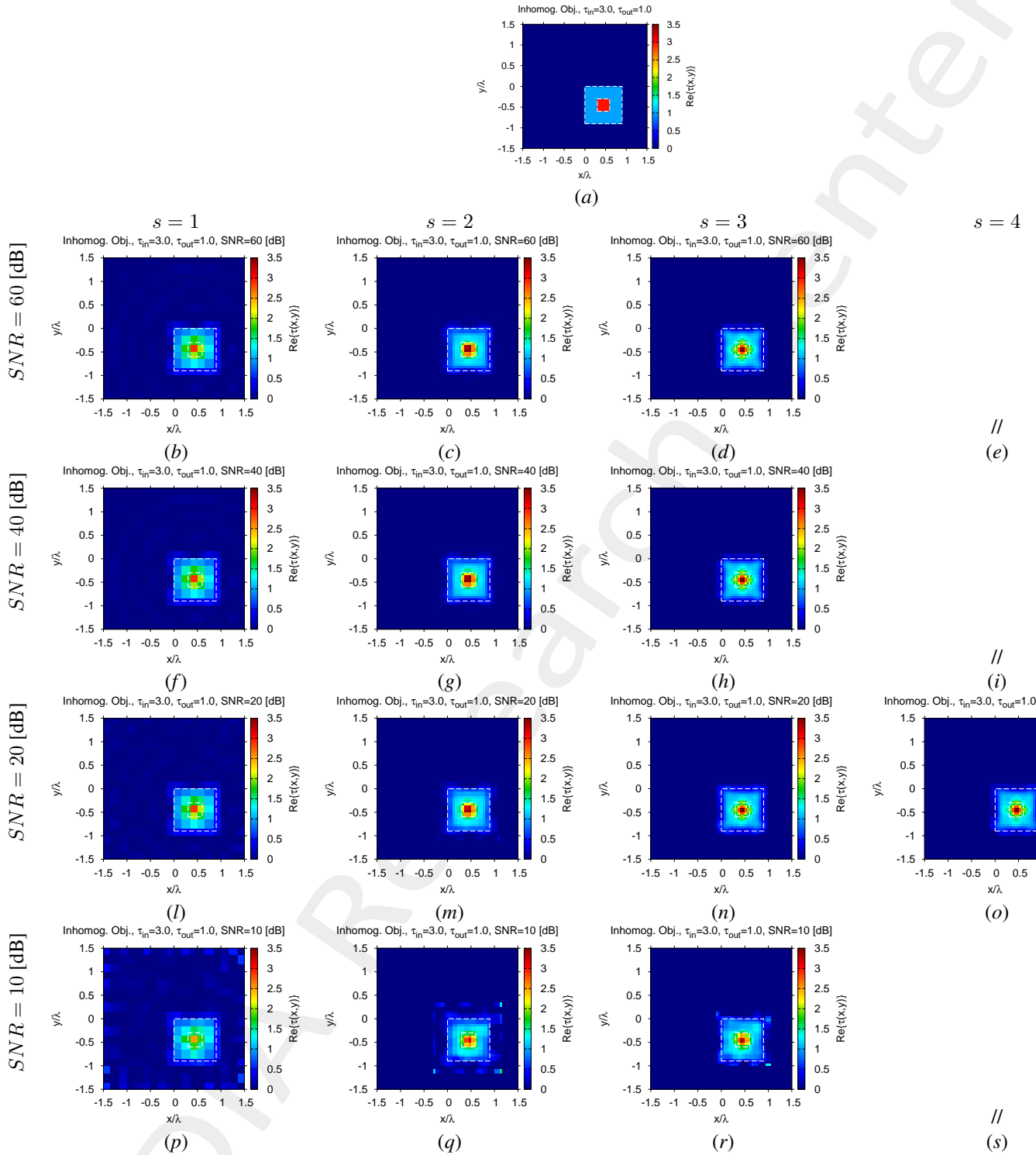


Figure 3: “Inhomogeneous Square” Profile, $\tau_{in} = 3.0$, $\tau_{out} = 1.0$ - (a) Actual and (b)-(i) intermediate retrieved contrast by the *IMSA – SOM – NIE* under several noise levels.

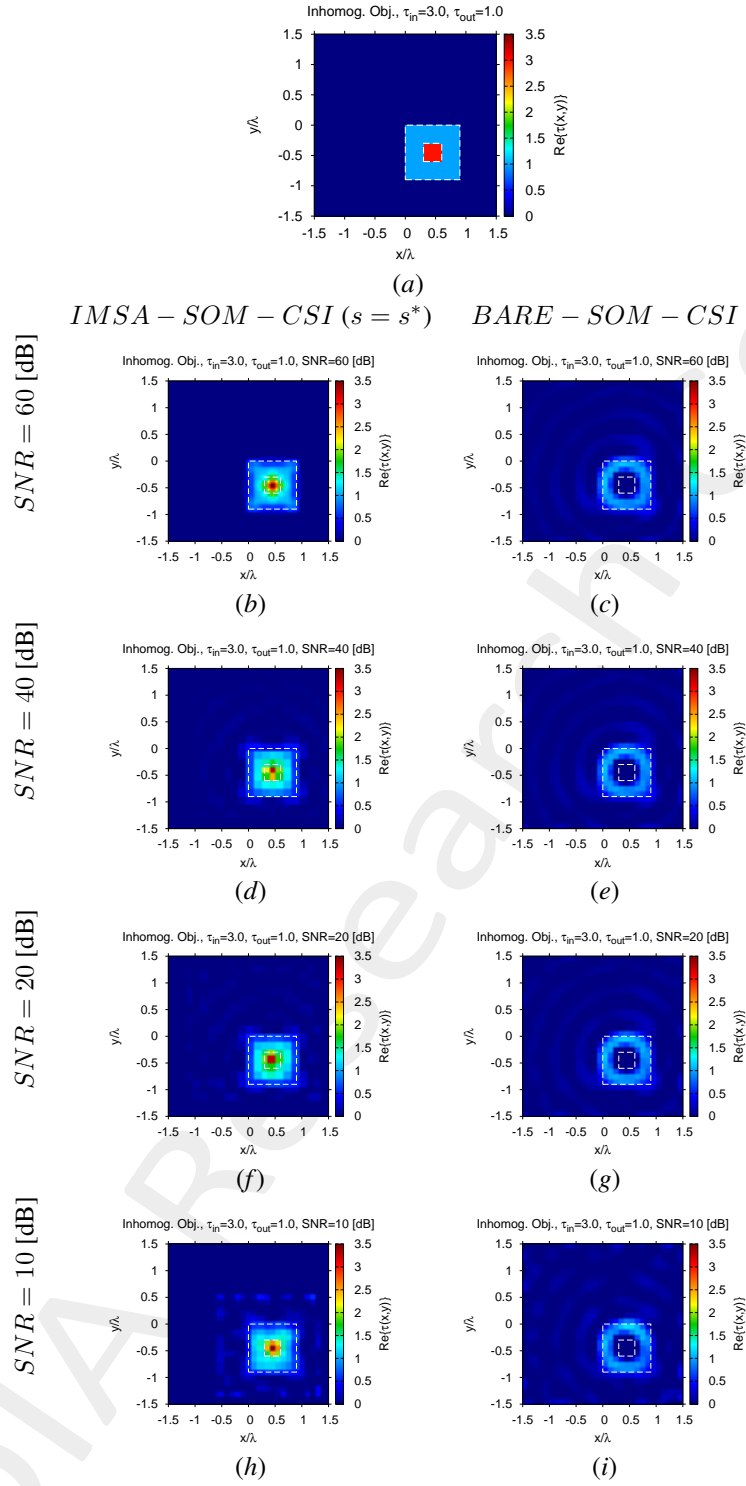


Figure 4: “Inhomogeneous Square” Profile, $\tau_{in} = 3.0$, $\tau_{out} = 1.0$ - (a) Actual and (b)-(i) retrieved contrast by the *IMSA – SOM – CSI* and *BARE – SOM – CSI* methods under several noise levels.

Reconstruction Errors vs. SNR

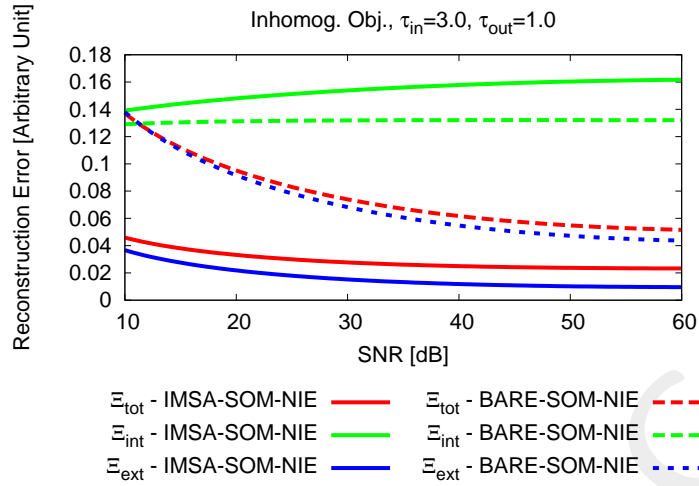


Figure 5: “Inhomogeneous Square” Profile, $\tau_{in} = 3.0, \tau_{out} = 1.0$ - Reconstruction errors for the *IMSA-SOM-NIE* and *BARE-SOM-NIE* methods.

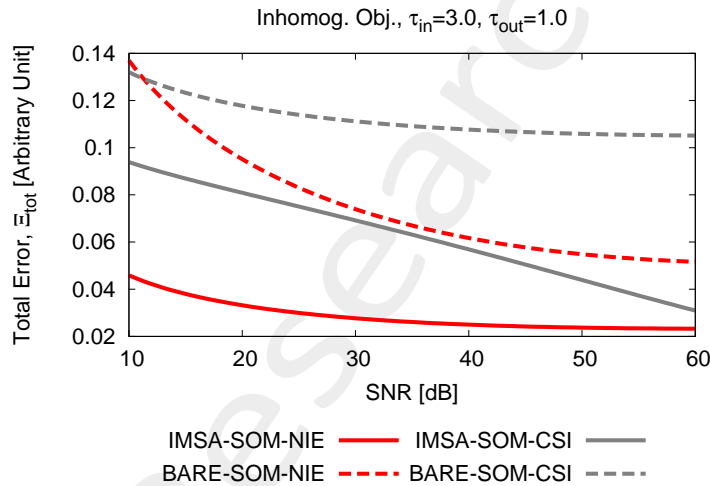


Figure 6: “Inhomogeneous Square” Profile, $\tau_{in} = 3.0, \tau_{out} = 1.0$ - Total error for *IMSA-SOM-NIE*, *BARE-SOM-NIE*, *IMSA-SOM-CSI*, and *BARE-SOM-CSI*.

2.2 Observations

- In general, the reported results in this section confirm the very good performance of the *IMSA-SOM-NIE* over state-of-the-art alternatives.

References

- [1] G. Oliveri, Y. Zhong, X. Chen, and A. Massa, "Multiresolution subspace-based optimization method for inverse scattering problems," *J. Opt. Soc. Am. A*, vol. 28, no. 10, pp. 2057-2069, Oct. 2011.
- [2] X. Ye, L. Poli, G. Oliveri, Y. Zhong, K. Agarwal, A. Massa, and X. Chen, "Multi-resolution subspace-based optimization method for solving three-dimensional inverse scattering problems," *J. Opt. Soc. Am. A*, vol. 32, no. 11, pp. 2218-2226, Nov. 2015.
- [3] T. Moriyama, G. Oliveri, M. Salucci, and T. Takenaka, "A multi-scaling forward-backward time-stepping method for microwave imaging," *IEICE Electronics Express*, vol. 11, no. 16, pp. 20140569(1-10), Aug. 2014.
- [4] N. Anselmi, G. Oliveri, M. Salucci, and A. Massa, "Wavelet-based compressive imaging of sparse targets," *IEEE Trans. Antennas Propag.*, vol. 63, no. 11, pp. 4889-4900, Nov. 2015.
- [5] M. Salucci, G. Oliveri, and A. Massa, "GPR prospecting through an inverse scattering frequency-hopping multi-focusing approach," *IEEE Trans. Geosci. Remote Sens.*, vol. 53, no. 12, pp. 6573-6592, Dec. 2015.
- [6] T. Moriyama, M. Salucci, T. Tanaka, and T. Takenaka, "Image reconstruction from total electric field data with no information on incident field," *J. Electromagn. Waves Appl.*, 2016.
- [7] M. Salucci, L. Poli, and A. Massa, "Advanced multi-frequency GPR data processing for non-linear deterministic imaging," *Signal Proc.*, vol. 132, pp. 306-318, Mar. 2017.
- [8] M. Salucci, L. Poli, N. Anselmi, and A. Massa, "Multifrequency particle swarm optimization for enhanced multiresolution GPR microwave imaging," *IEEE Trans. Geosci. Remote Sens.*, vol. 55, no. 3, pp. 1305- 1317, Mar. 2017.
- [9] N. Anselmi, G. Oliveri, M. A. Hannan, M. Salucci, and A. Massa, "Color compressive sensing imaging of arbitrary-shaped scatterers," *IEEE Trans. Microw. Theory Techn.*, vol. 65, no. 6, pp. 1986-1999, Jun. 2017.
- [10] G. Oliveri, M. Salucci, N. Anselmi, and A. Massa, "Compressive sensing as applied to inverse problems for imaging: theory, applications, current trends, and open challenges," *IEEE Antennas Propag. Mag.*, vol. 59, no. 5, pp. 34-46, Oct. 2017.
- [11] M. Salucci, A. Gelmini, L. Poli, G. Oliveri, and A. Massa, "Progressive compressive sensing for exploiting frequency-diversity in GPR imaging," *J. Electromagn. Waves Appl.*, vol. 32, no. 9, pp. 1164- 1193, 2018.
- [12] G. Oliveri, M. Salucci, and N. Anselmi, "Tomographic imaging of sparse low-contrast targets in harsh environments through matrix completion," *IEEE Trans. Microw. Theory Techn.*, vol. 66, no. 6, pp. 2714-2730, Jun. 2018.
- [13] M. Salucci, L. Poli, and G. Oliveri, "Full-vectorial 3D microwave imaging of sparse scatterers through a multi-task Bayesian compressive sensing approach," *J. Imaging*, vol. 5, no. 1, pp. 1-24, Jan. 2019.
- [14] M. Salucci, G. Oliveri, and A. Massa, "Real-time electrical impedance tomography of the human chest by means of a learning-by-examples method," *IEEE J. Electromagn., RF, Microw. Med. Biol.*, vol. 3, no. 2, pp. 88-96, Jun. 2019.

-
- [15] G. Oliveri, L. Poli, N. Anselmi, M. Salucci, and A. Massa, "Compressive sensing-based Born iterative method for tomographic imaging," *IEEE Trans. Microw. Theory Techn.*, vol. 67, no. 5, pp. 1753-1765, May 2019.
- [16] I. Merunka, A. Massa, D. Vrba, O. Fiser, M. Salucci, and J. Vrba, "Microwave tomography system for methodical testing of human brain stroke detection approaches," *Int. J. Antennas Propag.*, vol. 2019, ID 4074862, pp. 1-9, 2019.
- [17] Y. Zhong, M. Salucci, K. Xu, A. Polo, and A. Massa, "A multi-resolution contraction integral equation method for solving highly non-linear inverse scattering problems," *IEEE Trans. Microw. Theory Techn.*, vol. 68, no. 4, pp. 1234-1247, Apr. 2020.
- [18] M. Salucci, A. Polo, K. Xu, and Y. Zhong, "A multi-resolution computational method to solve highly non-linear inverse scattering problems," *Journal of Physics: Conference Series*, vol. 1476, pp. 1-6, 2020.
- [19] N. Anselmi, L. Poli, G. Oliveri, and A. Massa, "Iterative multi-resolution bayesian CS for microwave imaging," *IEEE Trans. Antennas Propag.*, vol. 66, no. 7, pp. 3665-3677, Jul. 2018.
- [20] G. Oliveri, P.-P. Ding, and L. Poli "3D crack detection in anisotropic layered media through a sparseness-regularized solver," *IEEE Antennas Wireless Propag. Lett.*, vol. 14, pp. 1031-1034, 2015.
- [21] L. Poli, G. Oliveri, P.-P. Ding, T. Moriyama, and A. Massa, "Multifrequency Bayesian compressive sensing methods for microwave imaging," *J. Opt. Soc. Am. A*, vol. 31, no. 11, pp. 2415-2428, 2014.
- [22] G. Oliveri, N. Anselmi, and A. Massa, "Compressive sensing imaging of non-sparse 2D scatterers by a total-variation approach within the Born approximation," *IEEE Trans. Antennas Propag.*, vol. 62, no. 10, pp. 5157-5170, Oct. 2014.